SAR, SA, and Temperature Variation in the Human Head Caused by IR-UWB Implants Operating at 4 GHz

Kasun M. S. Thotahewa, *Student Member, IEEE*, Jean-Michel Redouté, *Senior Member, IEEE*, and Mehmet Rasit Yuce, *Senior Member, IEEE*

***Abstract*—With the extensive use of wireless devices within or at close proximity to the human body, electromagnetic effects caused by the interaction between RF waves and human tissues need to be considered with paramount importance. The ultra-wideband (UWB) communication spectrum has recently been utilized in biotelemetry applications, such as neural recording, brain-computer interfaces, and physiological data monitoring requiring high data rate and low power. This paper reports the electromagnetic effects of head-implantable transmitting devices operating based on impulse radio UWB wireless technology. Simulations illustrate the performance of an implantable UWB antenna tuned to operate at 4 GHz with an −10-dB bandwidth of approximately 1 GHz when it is implanted in a human head model. Specific absorption rate (SAR), specific absorption (SA), and temperature increase are analyzed to compare the compliance of the transmitting device with international safety regulations. The frequency- and age-dependent nature of the tissue properties, such as relative permittivity, is taken into account. The SAR/SA variation of the human head is presented with varying input power, different antenna orientations, and different signal bandwidths. We also present the percentage of SAR variation for each tissue type in the head model used for the simulations.**

***Index Terms*—Electromagnetic exposure, impulse radio ultra-wideband (IR-UWB), specific absorption rate (SAR), ultra-wideband (UWB) antenna, wireless body area network (WBAN).**

I. Introduction

WIRELESS communication for implantable devices has drawn the attention of researchers in recent years due to the various advantages it possesses, such as minimizing restrictions in daily activities, facilitating less invasive surgical procedures, and offering remote control and monitoring [1]–[4]. With the extensive use of wireless devices within or at close proximity to the human body, electromagnetic effects caused by the interaction between RF waves and human tissues are of paramount importance. Specific absorption rate (SAR), which determines the amount of signal energy absorbed by the human body tissue, is used as the index for many standards to regulate the amount of exposure of the human body to electromagnetic radiation [5], [6]. Various regulatory bodies provide different assessment methods and different maximum allowable SAR limits for the human tissues that are exposed to electromagnetic signals. Regulations by the International Council on Non-Ionizing Radiation Protection (ICNIRP) standard limits the localized 10-g averaged SAR of the head to 2 W/kg for signals in the range of 10 kHz to 10 GHz [5]. The IEEE/ICES C95.1-2005 standard limits the 10-g averaged SAR value over a 6-min time period to 1.6 W/kg [6]. Additional regulations are applied for pulsed transmission schemes in order to prevent auditory effects. A 2-mJ/kg specific absorption (SA) averaged over 10-g tissue weight for a single pulse is applied by the ICNIRP standard, while 576 J/kg averaged over a 10-g tissue for a 6-min period is applied by the IEEE/ICES C95.1-2005 standard.

Studies have shown that a temperature increase in excess of 1 °C could prove harmful to the human body [5]. Many studies have been carried out in order to assess the effect of RF signals [7]–[15]. Most of the research in this area has been done based on on-body scenarios, where most of the signal propagation occurs through air interface before coming into contact with the body tissues [10]–[18]. Due to the increased use of implantable wireless devices where most of the electromagnetic wave propagation occurs within the human tissue, it is important to analyze the effects of those devices on the human body. Only a few studies that investigate the effect of in-body propagation of electromagnetic waves on human tissue are reported in the literature [7], [8].

With the emergence of new techniques to record physiological data such as neural recording systems [16], the need of high data-rate wireless transmission has become a key requirement for implantable devices. Impulse radio ultra-wideband (IR-UWB) can be identified as a technology that caters the need for high data rate while requiring low power consumption [17]. Ultra-wideband (UWB) signals are defined as signals having a fractional bandwidth larger than 0.2 or a bandwidth of at least 500 MHz. UWB is allowed to operate in the 0–960 MHz and 3.1–10-GHz bands with the effective isotopic radiated power (EIRP) is kept below −41.3 dBm/MHz [18]. An IR-UWB system transmits pulses with short duration to represent data [17]. IR-UWB is more popular in body-centric applications compared to other types of UWB signals, such as multiband UWB, due to its simplicity of implementation: for this reason

Manuscript received October 15, 2012; revised February 19, 2013; accepted February 22, 2013.

The authors are with the School of Electrical and Computer Systems Engineering, Monash University, Clayton 3800, Vic., Australia (e-mail: kasun.thotahewa@monash.edu; Mehmet.Yuce@monash.edu; jean-michel.redoute@monash.edu).

Color versions of one or more of the figures in this paper are available online at http://ieeexplore.ieee.org.

Digital Object Identifier 10.1109/TMTT.2013.2250515

and out of clarity, IR-UWB is referred to as UWB in the remainder of this paper unless mentioned otherwise. Due to the inherent advantages of UWB, such as low power consumption, a small form factor in circuits and antennas, and a high data rate, it is considered as a suitable wireless technology for implant data transmission.

As UWB communication becomes more prominent in high data-rate implant communication [17], [19], [20], it is important to investigate the electromagnetic effects caused by a UWB transmitter implanted in the human body. Several publications are found in the literature that have analyzed the effect of UWB on the human body based on on-body scenarios [12]–[15]. They investigate the SAR variation caused by a UWB transmitting source placed externally at a close proximity of the human body. While these results provide a general understanding about the electromagnetic effects caused by on-body propagation of UWB signals, the work in this paper looks into the effects caused by implanted UWB devices. Many reported studies used homogeneous human body models; hence, they do not depict the differences in properties of various types of tissue materials, which can significantly affect the results. Also, it should be noted that the SAR variation depends on antenna properties, such as directivity, orientation, and gain. A few reported studies demonstrate the effects of RF transmission from implantable devices inside the human body [7], [8], [21]. Some of them report the SAR variations caused by implantable devices operating at low-frequency bands such as Medical Implant Communication Service (MICS) and industrial–scientific–medical (ISM) bands [7], [8]. The work reported in [21] illustrates the SAR variation caused by an IR-UWB source inside the human stomach. The latter uses the finite-difference time-domain (FDTD) computation method, which discretizes the derivatives in Maxwell's curl equations [22] using finite differences. However, [21] has not considered an antenna model in the simulations: additionally, the Federal Communications Commission (FCC) regulations that govern the UWB indoor propagation are not taken into account.

This paper presents the electromagnetic and thermal effects of IR-UWB transmission from a brain implant. We used a complex head model to simulate the combination of tissue materials present in the head. An implantable antenna working at UWB frequencies is used as the source of the UWB signals. The 4-Cole Cole model is used in order to consider the dispersive nature of the tissue materials at these high frequencies. Also, the effect of human age is considered when calculating the tissue properties such as relative permittivity. An IR-UWB pulse operating at a center frequency of 4 GHz and a bandwidth of 1 GHz has been chosen as the excitation to the antenna. This range is selected so that the UWB spectrum has minimum interference from other wireless technologies, such as 5-GHz Wi-Fi. The simulations are conducted in CST Studio [23], which has been recognized by the FCC as a suitable simulation tool for SAR calculations.

This paper is organized as follows. Section II describes the simulation methods and models such as tissue material parameterization methods, the SAR calculation model, and the use of the bio heat equation to obtain the temperature-related results. Section III presents SAR, SA, and temperature variation simulation results in terms of signal bandwidth, body tissue type, antenna orientation, and power level. Section IV concludes this paper.

II. Simulation Models and Methods

A. Effect of Human Tissue Properties on SAR

A compilation of experimental and theoretical results on human tissue property variation depending on the incident frequency provided in [24] proves that the former behaves differently at different incident frequencies. This is due to a property known as dielectric dispersion. The SAR value for a certain material subjected to an electromagnetic field can be calculated by (1) as follows [25]:

$$\mathrm{SAR} = \frac{1}{2}\frac{\sigma}{\rho}|E|^2 \tag{1}$$

where E is the root mean square (rms) electric field strength, ρ is the mass density (in kg/m^3), and σ is the conductivity of the tissue. The electric field and the magnetic field in the frequency domain can be described from Maxwell's curl equations in the frequency domain as follows:

$$\nabla \times \boldsymbol{E}(\boldsymbol{\omega}) = -j\omega\mu\boldsymbol{H}(\boldsymbol{\omega}) \tag{2}$$

$$\nabla \times \boldsymbol{H}(\boldsymbol{\omega}) = j\omega\varepsilon_0\varepsilon_r^{'}(\omega)\boldsymbol{E}(\boldsymbol{\omega}) \tag{3}$$

where $j = \sqrt{-1}$ is the imaginary unit, ω is the angular frequency, $\boldsymbol{E}(\boldsymbol{\omega})$ and $\boldsymbol{H}(\boldsymbol{\omega})$ are time–harmonic electric and magnetic fields, μ is the permeability, ε_0 is the free-space permittivity, and $\varepsilon_r^{'}(\omega)$ is the frequency-dependent complex relative permittivity. Due to the dependency of the electric field on $\varepsilon_r^{'}(\omega)$, the SAR variation inherently depends on the relative permittivity of the material, which itself depends on the incident frequency of the electromagnetic signal. The behavior of the complex relative permittivity for different tissue types differs from each other, especially at higher frequency ranges such as UWB. Hence, it is not advised to use straightforward homogeneous body models to simulate the electromagnetic effects at higher frequencies. The simulations presented in this paper use the CST Studio voxel head model, which is a head model consisting of a mixture of tissue materials such as brain, bone, fat, and skin. It also takes blood flow into account for thermal calculations.

The frequency-dependent dielectric permittivity can be expressed as [26]

$$\varepsilon_r^{'}(\omega) = \varepsilon^{'} - j\varepsilon'' = \varepsilon^{'} - j\frac{\sigma}{\varepsilon_0\omega} = \varepsilon^{'}\left(1 - j\frac{1}{\omega\tau}\right) \tag{4}$$

where $\varepsilon^{'}$ is the relative permittivity of the tissue material, ε'' is the out of phase loss factor, which can be expressed as $\varepsilon'' = (\sigma)/(\varepsilon_0\omega)$, and $\tau = (\varepsilon_0\varepsilon^{'})/(\sigma)$ is the relaxation time constant. In the expression for ε'', σ represents the total conductivity of the material, which might be partially attributed by frequency-dependent ionic conductivity σ_i, $\varepsilon_0 = 8.85 \times 10^{-12}$ F/m is the permittivity of the free space, and ω is the angular frequency. Based on this equation, Gabriel *et al.* have proposed a method

of evaluating the frequency-dependent relative permittivity of a material by so called 4-Cole Cole model approximation given in the following equation [27]:

$$\varepsilon_r^{'}(\omega) = \varepsilon_\infty + \sum_{n=1}^{4} \frac{\Delta\varepsilon_n}{1 + (j\omega\tau_n)^{1-\alpha_n}} + \frac{\sigma_i}{j\omega\varepsilon_0} \tag{5}$$

where ε_∞ is the permittivity when $\omega \to \infty$ (permittivity in terahertz frequencies in practical scenarios), $\Delta\varepsilon_n$ is the change in the permittivity in a specified frequency range during nth iteration, τ_n is the relaxation time during the nth iteration, α_n is the nth iteration of the distribution parameter, which is a measure of the broadening of dispersion, and σ_i is the static ionic conductivity. Due to the high computational complexity involved when calculating the SAR in the time domain, for example, when using the FDTD method, most of the literature available for SAR variation in body tissues is using an approximation method such as the Debye approximation [9] or the so-called $4 \times L$ Cole Cole approximation [21] instead of the more accurate 4-Cole Cole model of tissue properties. This is mainly due to the fact that obtaining a time-domain expression for $\varepsilon_r^{'}(\omega)$ for $0 < \alpha_n < 1$ is computationally intensive. The approach followed in this paper has been to compute the SAR in the frequency domain, which enables to use the more accurate 4-Cole Cole approximation in the obtained calculations.

Apart from the frequency-dependent dispersive nature of the tissue materials, the human age affects the electromagnetic behavior of body tissues. This is mainly due to the change in the water content of tissue with age [28], [29]. Methods presented in [30] follow the Lichtenecker's exponential law for the complex permittivity based on the water content of human tissue materials [31]. According to the information given in [29], the relative permittivity of any tissue material (i.e., real part of the complex relative permittivity [$\varepsilon^{'}$ in (4)]) can be calculated as

$$\varepsilon^{'} = \varepsilon_w^{\beta} \varepsilon_t^{1-\beta} \tag{6}$$

where ε_W is the permittivity of water, ε_t is the age-independent relative permittivity of the tissue organic material, and β is the hydrate rate for the tissue material. β can be expressed as $\beta = \rho \cdot \mathrm{TBW}$, where $\mathrm{TBW} = 784 - 241 \cdot e^{\{-[(\ln((\mathrm{AGE})/(55)))/(6.9589)]^2\}}$ is the total body water index (AGE is the age of the tissues sample in years) [30], [32]. After some primary operations, the frequency-dependent complex permittivity for body tissues can be expressed as follows [30]:

$$\varepsilon_r^{'}(\omega) = \varepsilon_w^{\frac{\beta-\beta_A}{1-\beta_A}} \varepsilon_A^{\frac{1-\beta}{1-\beta_A}} \left(1 - j\frac{1}{\omega\tau}\right) \tag{7}$$

where ε_A is the age-dependent relative permittivity of a reference adult tissue material, which can be expressed as $\varepsilon_A = \varepsilon_w^{\beta_A} \varepsilon_t^{1-\beta_A}$ by replacing $\varepsilon^{'} = \varepsilon_A$ in (6) (for present simulations, the tissue parameters of a 55-year-old adult are used as reference) and β_A is the hydrate rate for adult tissues [all other parameters are described in (4) and (6)]. By using the 4-Cole Cole approximation in combination with the age-related tissue parameter approximations, it is possible to characterize the human tissue properties with sufficient precision. This approach has been utilized in this study. This study also considers the relative permittivity variation of water depending on the incident frequency instead of the constant value used in [30] for age-related calculations. Fig. 1 depicts the variation of $\varepsilon^{'}$ and ε'' as a function of frequency for the brain tissue material of a child of seven years and a male of 55 years. The basic set of tissue parameters required for the calculation (e.g., $\tau_1 - \tau_4$,, $\Delta\varepsilon_1 - \Delta\varepsilon_4$, and $\alpha_1 - \alpha_4$) of the 4-Cole Cole approximation is taken from [24]. It should be observed that while $\varepsilon^{'}$ depends on the variation of the tissue water content with age, ε'' is largely age independent as the latter is determined by the conductivity (σ). This can be seen in Fig. 1.

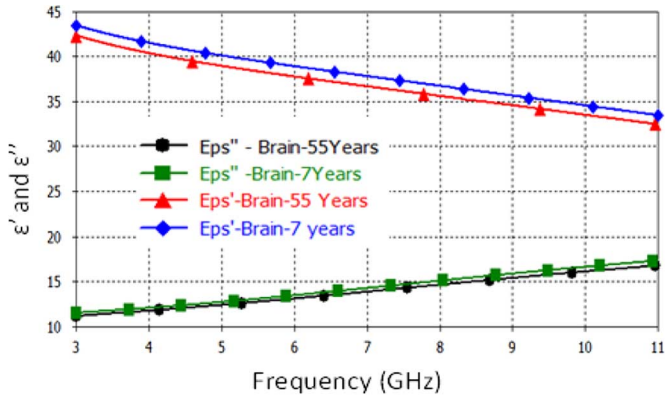

Fig. 1. Simulated variation of $\varepsilon^{'}$ and ε'' in the UWB frequency range.

B. SAR Calculation Method

The finite integration technique (FIT) is used as the volume discretization approach for the described simulations. This technique is used to calculate the absorption loss of the body tissues by discretizing the Maxwell's curl equations in a specified domain [33]. The discretizing volume element is chosen to be cubic, and appropriate boundary conditions are applied in order to define the power absorbed within that cube. Further information on the FIT model can be found in [33] and [34].

SAR is defined as the power absorbed by the mass contained within that discretized volume element shown in (8) as follows [35]:

$$\mathrm{SAR} = \frac{d\left(\frac{\Delta W}{\rho dV}\right)}{dt} \tag{8}$$

where ΔW is the mass of the discretized volume element and dV is its incremental volume. Present simulations use an IR-UWB signal pulse as the excitation signal, and are conducted in order to calculate the 10-g averaged SAR so as to compare it with the ICNIRP specifications for pulse transmission [5]. The maximum SAR within the 10 g of tissue averaging volume is taken into consideration in order to demonstrate the worst case scenario. The SA per pulse, which is being used to introduce additional limitations for pulsed transmissions in the ICNIRP limitations, is computed using

$$\mathrm{SA} = \mathrm{SAR} \times T_p \tag{9}$$

where T_p is the pulse duration.

It should be noted that heat sources such as the electronic components used in the implanted circuitry also affect the SAR variation in the body tissues. The influence of these heat sources are not considered in the performed simulations since the main purpose of this work is to determine the effect of the IR-UWB electromagnetic field on the SAR variations.

C. Temperature Variation Based on Bio Heat Model

When exposed to an electromagnetic field, the absorbed power by the body tissues causes a temperature increase. A temperature increase exceeding 1 °C–2 °C in the human body tissue can cause adverse health effects, such as a heat stroke [39]. In addition to the study of SAR variations, this paper also analyses the temperature variation in the human head when it is exposed to IR-UWB transmission from an implanted transmitter. The temperature of the body tissues is modeled using the following bio heat equation in (10) [37]:

$$Cp\frac{\delta T}{\delta t} = \nabla \cdot (k\nabla T) + \rho \cdot \mathrm{SAR} + A - B(T - T_b) \quad (10)$$

where K is the thermal conductivity, Cp denotes the specific heat, A is the basal metabolic rate, B is the term associated with blood perfusion, ρ is the tissue density in (kg)/(m^3), and $\nabla \cdot (k\nabla T)$ represents the thermal spatial diffusion term for heat transfer through conduction at temperature T in degrees Celsius.

The bio heat equation in (10) is solved with the boundary conditions given in (11), namely,

$$K\frac{\delta T}{\delta n} = -h \cdot (T - T_a) \quad (11)$$

where T_a is the temperature of the surrounding environment, n is the unit vector normal to the surface of interest, and h is the convection coefficient for heat exchange with the external environment.

The human body tries to regulate its core temperature by various mechanisms in order to keep it at approximately 37 °C. The effect of thermo regulatory mechanisms causes the tissue specific basal metabolic rate (A) and blood perfusion coefficient (B) in (10) to exhibit a dependency on body temperature rather than being a constant value. The basal metabolic rate is modeled using (12) [38],

$$A = 1.1A_0^{T-T_0} \quad (12)$$

where T_o is the basal temperature and A_o is the basal metabolic rate of the tissue.

The blood perfusion is only dependent on the local blood temperature. Variation of the blood perfusion with the temperature is obtained using the set of equations presented in [39]. All the heat-related parameters for the calculation of temperature variation are obtained from [39].

D. Implantable Antenna Model and Impedance Matching

The variation of the SAR is highly dependent on the antenna parameters, such as directivity and gain. The UWB antenna considered in this paper was modeled on the work presented in [40]. The dimensions of the antenna are 23.7 × 9 × 1.27 mm, which

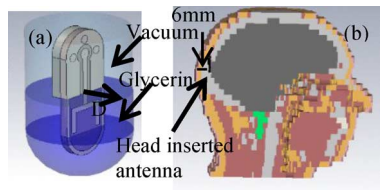

Fig. 2. (a) IR-UWB antenna. (b) Insertion in the head.

are reasonable values to be used within a neural implant. The antenna is tuned to operate at around 4 GHz with a bandwidth of 1 GHz, which fulfills the bandwidth requirement imposed by the FCC for UWB communication. The antenna was inserted inside a capsule-shaped casing with a negligible thickness compared to the antenna dimensions, in order to prevent direct contact between antenna radiating elements and the neighboring tissue. Using an insulating material with a relative permittivity close to that of the surrounding tissue material between the latter and the antenna increases the impedance-matching characteristics [40]. Glycerin, which has a relative permittivity value of 50, is chosen as the appropriate insulating material when the antenna is surrounded mainly by the brain tissue, which has a relative permittivity of around 40 at 4 GHz. The designed antenna is half embedded inside the insulating material, where only the lower half of the antenna is immersed in glycerin. This improves the impedance-matching characteristics in the implant [40]. The antenna is placed at 6-mm distance from the surface of the head. Fig. 2 depicts how this antenna model is used alongside the CST voxel head model in order to perform present simulations.

The dimensions of the antenna capsule are significant to achieve a proper impedance matching characteristic [40]. Through simulation-based optimization, the optimum value for the radius of the capsule (D) was obtained to be 5 mm for the head-implanted antenna, which is indicated in Fig. 2. For most of the simulation scenarios, the antenna is inserted in the head such that the main far-field lobe of the antenna is pointing outwards from the brain. This is a realistic data communication scenario due to the fact that the main lobe of the transmitting antenna far field is used to excite the antenna of the receiver that is placed outside the human head. However, for the purpose of comparison, simulations for the worst case scenario where the antenna main lobe is pointing toward the brain have been performed as well.

S-parameter characteristics and antenna gain/directivity far-field characteristics are presented in Figs. 3 and 4, respectively. It should be noted that the near-field characteristic of the antenna predominantly affects the SAR and the thermal behavior of the body tissues. The near-field simulation characteristics are shown in Section III. Although the far-field stretches outside of the brain, and therefore does not influence the SAR, the far-field characteristics are shown in order to compare the antenna performance in different scenarios as well as to get an idea about the direction in which the maximum power transfer is radiated by the antenna.

The gain and total efficiency values obtained for the brain implant are comparable with the values reported in [40]. In the scenario where the antenna main lobe is directed toward the brain,

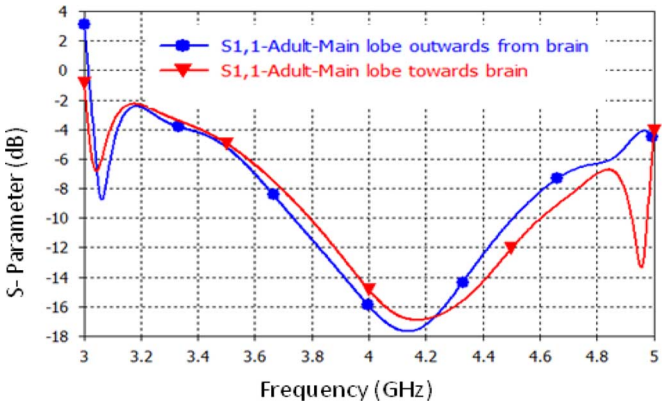

Fig. 3. Simulated $S11$ for the two different implant orientations.

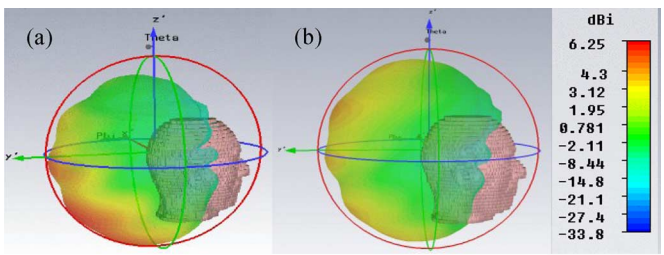

Maximum Directivity=6.25 dBi
Total Efficiency= 0.0094
Gain= -13.9 dBi

Maximum Directivity=4.48 dBi
Total Efficiency= 0.005
Gain=-18.4 dBi

Fig. 4. Simulated directivity of the implanted antenna at 4 GHz. (a) Antenna radiating outwards of the adult brain. (b) Antenna radiating toward the adult brain (the simulated total antenna efficiency and antenna gain for each orientation is given under the directivity plots).

the antenna sidelobe is considered for the calculation of gain and directivity. It can be seen that the gain in this scenario is lower than in the scenario where the antenna main lobe is directed outwards of the brain. For the calculation of gain and total efficiency values, the power loss due to tissue absorption is considered [40]; hence, it can be used to assess the power radiated into free space resulting from a specified excitation pulse, which is applied to the antenna.

III. Results and Discussion

A. IR-UWB Excitation Pulse

An IR-UWB signal centered at 4 GHz with a bandwidth of 1 GHz has been applied to the designed UWB antenna. Initially, an FCC regulated IR-UWB pulse [18] has been used in order to investigate SAR and temperature effects. The use of an FCC regulated UWB pulse for excitation is useful to compare the obtained results with the results available in the literature. The pulse duration is 2 ns. These pulses are obtained from a pulse train with a period of 50 ns.

The pulse amplitude of that signal has been adjusted ensuring that the input power to the antenna falls within the FCC regulated power spectrum. The FCC regulated power input to the antenna, along with its power spectral density and the

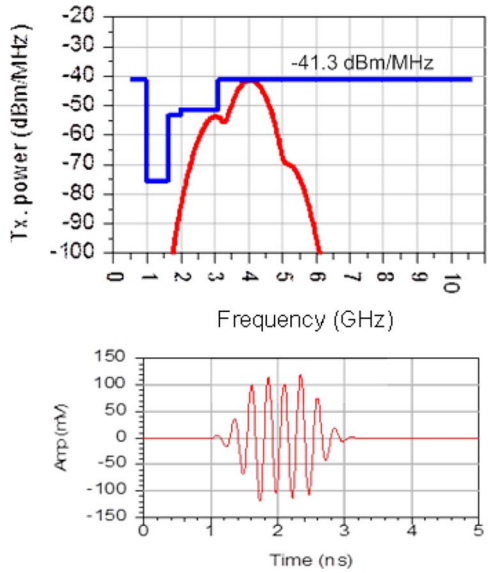

Fig. 5. FCC regulated input pulse and its power spectrum.

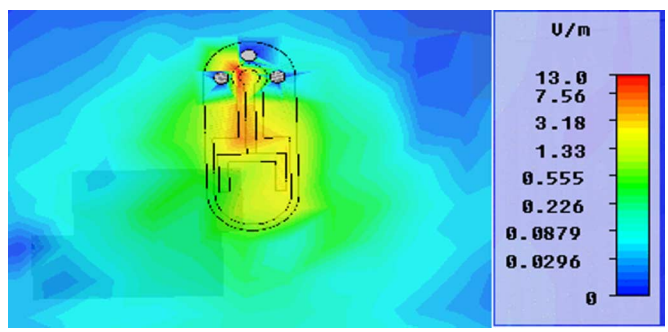

Fig. 6. Magnitude of the electric field generated by the antenna at 4 GHz and phase $= 112.5°$ on the X–Y-plane at a distance of $Z = 0.1$ mm, when excited by a FCC regulated IR-UWB pulse.

FCC regulated spectrum limit, is shown in Fig. 5. The total power contained in that pulse within the 3.5–4.5-GHz band is calculated as 0.0024 mW. The power calculation is done by integrating the power spectrum of the UWB pulse in the frequency range of 3.5–4.5 GHz using the simulation software. Simulations recorded negative gain values of the antenna after the tissue absorption: this means that the signal emitted in free space is lower than the radiated power from the implanted antenna. Hence, it is possible to excite the antenna with a signal power higher than the outdoor allowable -41.3-dBm/MHz power limit by increasing the excitation signal amplitude such that the power emitted to the free space after tissue absorption lies within the FCC regulations. Simulations in order to analyze the effect of this kind of manipulation on the SAR and temperature variation were conducted as well. The near electric field of the implanted antenna has been found to be the main contributor to the SAR variation in the surrounding tissue. The generated near field of the implanted antenna, when it is excited by the FCC regulated pulse depicted in Fig. 5, is shown in Fig. 6.

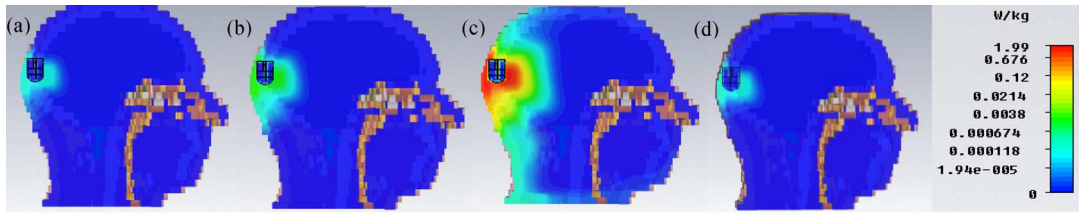

Fig. 7. Side view of the simulated 10-g averaged SAR variation in the adult voxel head model (a)–(c) when the antenna main lobe is situated outwards of the brain for the peak spectral power limits of: (a) −41.3 dBm/MHz and (b) −27.4 dBm/MHz and (c) 0.9 dBm/MHz and (d) when the antenna main lobe is situated toward the brain for the peak spectral power limit of −41.3 dBm/MHz.

B. SAR Variation

1) SAR Variation for Different Input Signal Power Levels: Using the developed simulation models, the 10-g averaged SAR variations for three different input power values have been analyzed in a 30-year-old adult head (Fig. 7). The first scenario uses a FCC regulated IR-UWB pulse, which lies within the specified −41.3-dBm/MHz limit, depicted in Fig. 5. The second scenario is obtained by considering the results in Fig. 4(a): it can be observed in the latter figure that the resulting maximum antenna gain is −13.9 dBi. This means that if a pulse with a peak power limit of 13.9 dB higher than the FCC regulated peak power limit of −41.3 dBm/MHz is used as the input to the implanted antenna, the radiation in free space will lie at the FCC limit. This corresponds to an input pulse with peak spectral limit of −27.4 dBm/MHz. In the third scenario, an IR-UWB pulse that causes a maximum SAR of 2 W/kg is used: the latter value is specified as the maximum allowable SAR limit by the ICNIRP regulations. The SA in previous three scenarios is also calculated for a pulsewidth of 2 ns in order to form a comparison with the ICNIRP special regulations for pulse transmissions. The results depicted in Fig. 7 show that the SAR and SA values obtained for the first and second scenario are well within the ICNIRP regulation limit for a single pulse of 2 W/kg and 2 mJ/kg, respectively. This is due to the very small power contained in the signal (a total in-band accepted power of 0.0024 mW in scenario 1 and 0.0504 mW in scenario 2 considering a bandwidth of 1 GHz). It should be noted that the color scale is set to reflect the maximum SAR in all the scenarios, and is logarithmically marked to yield an acceptable resolution for low SAR values. The SAR variation in scenario three uses a signal, which lies within a peak limit of 0.9 dBm/MHz for an amplitude increased version of the pulse shown in Fig. 5, but violates the FCC regulations for IR-UWB indoor propagation.

There are only a few studies found in the literature that analyze the SA/SAR variation for UWB-based head implants. Results shown in [11] assume a maximum total delivered power of 1 W to the antenna, and hence, ignores the limitation applied by the FCC with regard to UWB pulses. It has recorded a maximum SA of 10 pJ/kg in the human head. The results shown in [41] are based on a simple tissue model for the human head. It also uses a total delivered power of 1 W to the antenna and a UWB antenna bandwidth of 7 GHz. The results show a 1-g averaged SAR variation in excess of 100 W/kg, which is above the SAR regulation limits. The work carried out in [42] analyzes the SAR variation caused by a head-implanted UWB antenna using a simplified three-layer head tissue model with the antenna implanted underneath the skin. The results show a 1-g averaged SAR within a 1.6-W/kg limit for delivered power of 1 mW to the antenna. The FCC regulations are not considered in the simulations. The study in [9] reports results similar to values shown in Fig. 7(b). The authors have used the FCC regulated UWB signal with its power adjusted for tissue absorption losses as the excitation source for calculating the SAR values for an on-body scenario. The obtained SAR results in this paper are marginally higher than those reported in [9] mainly because this paper considers an implanted transmitter, while [9] considers an on-body device. SAR analysis for head-implanted narrowband antennas are reported in [43] and [44], but the results are not comparable with this work due to the difference in the excitation signals.

2) SAR Variation Depending on Antenna Orientation: The effect of the antenna orientation is considered in this paragraph. Two cases are considered, depending on whether the main lobe is situated outwards or inwards of the brain. In the former case, the SAR variation is obtained by placing the antenna main lobe outwards of the brain for an adult head model aged to 30 years. In the latter case, the antenna main lobe radiates toward the brain. These two scenarios are used to represent various possible applications of wireless transmission in the head. For both cases, an FCC regulated IR-UWB pulse has been considered. The results obtained are shown in Fig. 7(a) and (d). The SAR value for the adult head model with the antenna main lobe pointing toward the brain is 0.007 mW/kg higher than its counterpart shown in Fig. 7(a). This is a comparatively negligible value and is caused by the different orientations in the near field.

3) SAR Variation in Different Tissue Materials in the Human Head: The SAR variation percentages for all the tissue types involved in the simulation of the IR-UWB signal with a peak power limit of −27.4 dBm/MHz and when the antenna main lobe is located outwards from the brain are shown in Fig. 8: this case corresponds to the simulation depicted in Fig. 7(c). The mass percentage of each tissue type is indicated alongside the SAR. The total SAR recorded for this scenario is 0.102 mW/kg, and the total mass of the head tissue is equal to 4.766 kg. It should be noted that the total SAR is calculated by dividing the total absorbed power by the corresponding tissue masses, unlike the calculation of the 10-g averaged SAR where local averaging

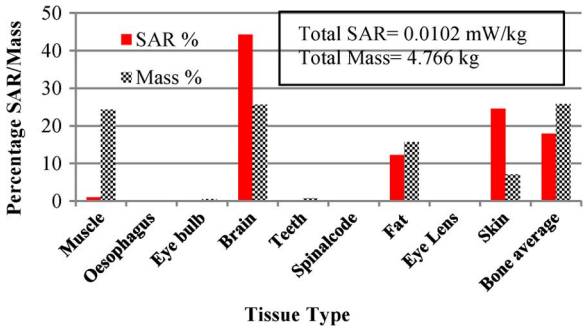

Fig. 8. SAR percentages and mass variation of tissue considered in the simulation.

TABLE I
SAR VARIATION WITH PULSE BANDWIDTH

Bandwidth (MHz)	100	250	500	750	1000
Pulse width (ns)	17	6.5	3.5	2.5	2
Total power in the pulse (mW)	3.164×10^{-4}	7.798×10^{-4}	0.0015	0.002	0.0024
Max SAR (mW/kg)	0.0153	0.0378	0.0727	0.097	0.166
Max SA (pJ/kg)	0.2601	0.2457	0.25445	0.2425	0.332

over a 10 g of tissue material is considered and the maximal value is retained.

As illustrated in Fig. 8, brain, fat, skin, and bone can be considered as tissue types with considerably high SAR percentage values. The maximum SAR percentages are recorded for the brain tissue. This is due to the fact that most of the radiated power from the antenna sidelobe is directed toward the latter. The SAR percentage for the skin is relatively high considering its lower mass percentage: this is mainly due to the high water content in the former's tissue. The low water content in the bone tissue causes a comparatively low SAR value despite its comparatively high mass percentage.

4) SAR Variation With the Signal Bandwidth: Simulations are conducted to show the dependency of the SAR on the signal bandwidth: IR-UWB pulses with different bandwidths, centered at 4 GHz, are used. The pulses are generated by passing a square wave through a bandpass filter of appropriate bandwidth followed by an amplification stage that adjusts the pulse amplitudes such that their spectrum falls within the FCC mask. The change in pulse widths for the corresponding bandwidth is tabulated in Table I alongside the total power contained in the pulses and the maximum SAR values obtained for each bandwidth. It can be observed from the results that the SAR variation has a great dependency on the signal bandwidth. This is caused by the variation in the in-band power levels for different bandwidths and an increased power absorption in the tissue at higher frequencies. The variation of SA depends on both the SAR value and the pulse width. Due to the decrease in pulsewidth with the increasing bandwidth, the SA values remain fairly constant.

C. Temperature Variation

Simulations using the same input power scenarios as reported in Fig. 7(a)–(c) are used to obtain the corresponding temperature variations. The bio heat equation considers the variation of basal metabolic rate and blood perfusion. Due to the short duration of the excitation pulse, the heat conduction that occurs through sweating is assumed to be negligible. The temperature increase is obtained after the steady state is achieved. The initial body temperature is considered to be 37 °C. Fig. 9 depicts the obtained temperature variations.

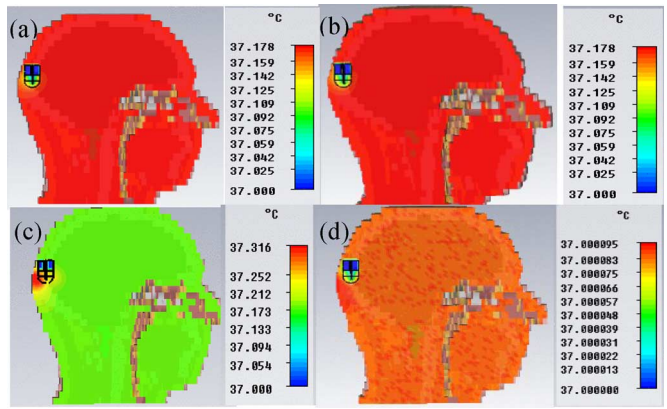

Fig. 9. Simulated temperature variation for a signal with peak spectral power limits of: (a) −41.3 dBm/MHz, (b) −27.4 dBm/MHz, and (c) 0.9 dBm/MHz using bio heat equation (d) −27.4 dBm/MHz without using bio heat equation.

It can be seen in Fig. 9(a) and (b) that the temperature of the whole head is increased from the initial temperature of 37 °C to 37.178 °C. It is not possible to see a significant temperature difference between the tissues at a close proximity to the antenna and those that are at a considerable distance from the antenna. This can be explained as follows. The temperature of the head as a whole increases up to 37.178 °C due to the metabolic activities in the tissues. The input powers to the antennas for cases shown in Fig. 9(a) and (b) are not large enough to cause a significant temperature increase due to the power absorption by the tissues. The temperature increases caused by the small radiated powers in these two cases are small enough to be regulated by the blood perfusion inside the head. This explanation is further justified by the results shown in Fig. 9(c) and (d). The power delivered to the antenna for the case in Fig. 9(c) is higher than that of Fig. 9(a) and (b). The high delivered power to the antenna generates a large enough electric field that causes high power absorption in the tissues. As a result, this high power absorption causes a considerable temperature increase in the tissues. It is clearly visible in Fig. 9(c) that the temperature of the tissues closer to the antenna are higher (a maximum of 37.316 °C is recorded in the simulations) than the temperature increase due to the metabolic activities in rest of the tissues (i.e., 37.178 °C). The simulations resulted in Fig. 9(d) ignore the heat generation from the metabolic activities and it does not regulate the temperature through blood perfusion. The power of the excitation pulse is set to fall within the −27.4-dBm/MHz spectral mask, which is similar to that of Fig. 9(b). There is an observed negligible temperature increase near the antenna for this case. This proves that the reason for the absence of a visible temperature increase for the simulations of Fig. 9(b) is blood perfusion. As can be observed in all four figures, the temperature in the glycerin insertion region of the antenna is lower than the temperature of the surrounding tissue that is heated up by metabolic activities.

This is due to the fact that the initial temperature of glycerin was lower than the body temperature for the simulations.

IV. Conclusion

This paper has described the electromagnetic exposure effects of a UWB implanted device targeted at applications such as neural recording and brain computer interfaces. The FCC regulations for the outdoor transmit power for UWB communication determines the maximum allowable signal power from an implanted IR-UWB-based transmitter. The SAR and SA results for the maximum peak power limits of -41.3 and -27.4 dBm/MHz lie well within the ICNIRP regulated limits. The temperature increase due to the exposure of the head tissues to the IR-UWB electromagnetic field at those peak power limits is found to be well within the control of thermal regulatory mechanisms of the human body. It was also observed that the SAR is highly dependent on the bandwidth of the IR-UWB signal. This study also showed that it is possible to excite the antenna with a signal power higher than the outdoor allowable -41.3-dBm/MHz power limit. It is found that a pulse with a peak power limit of 13.9 dB higher than the FCC regulated peak power can be utilized without violating SAR/SA limits, as well as the outdoor FCC regulations for this particular model.

References

[1] N. Gopalsami, I. Osorio, S. Kulikov, S. Buyko, A. Martynov, and A. C. Raptis, "SAW microsensor brain implant for prediction and monitoring of seizures," *IEEE Sens. J.*, vol. 7, no. 7, pp. 977–982, Jul. 2007.

[2] A. V. Nurmikko, J. P. Donoghue, L. R. Hochberg, W. R. Patterson, Y.-K. Song, C. W. Bull, D. A. Borton, F. Laiwalla, S. Park, Y. Ming, and J. Aceros, "Listening to brain microcircuits for interfacing with external world," in *Proc. IEEE Progr. Wireless Implantable Microelectron. Neuroeng. Devices*, Mar. 2010, vol. 98, no. 3, pp. 375–388.

[3] C. Cavallotti, M. Piccigallo, E. Susilo, P. Valdastri, A. Menciassi, and P. Dario, "An integrated vision system with autofocus for wireless capsular endoscopy," *Sens. Actuators A, Phys.*, vol. 156, no. 1, pp. 72–78, 2009.

[4] X. Chen, X. Zhang, L. Zhang, X. Li, N. Qi, H. Jiang, and Z. Wang;, "A wireless capsule endoscope system with low-power controlling and processing ASIC," *IEEE Trans. Biomed. Circuits Syst.*, vol. 3, no. 1, pp. 11–22, Feb. 2009.

[5] "Guidelines for limiting to time varying electric, magnetic, and electromagnetic fields (up to 300 GHz)," ICNIRP, Oberschleissheim, Germany, 1997.

[6] *IEEE Standard for Safety Levels With Respect to Human Exposure to Radio Frequency Electromagnetic Fields, 3 kHz to 300 GHz IEEE*, IEEE Standard C95.1-2005, 2005.

[7] P. Soontornpipit, "Effects of radiation and SAR from wireless implanted medical devices on the human body," *J. Med. Assoc. Thailand*, vol. 95, no. 2, pp. 189–197, 2012.

[8] L. Xu, M. Q. H. Meng, H. Ren, and Y. Chan, "Radiation characteristics of ingestible wireless devices in human intestine following radio frequency exposure at 430, 800, 1200, and 2400 MHz," *IEEE Trans. Antennas Propag.*, vol. 57, no. 8, pp. 2418–2428, Aug. 2009.

[9] Q. Wang and J. Wang, "SA/SAR analysis for multiple UWB pulse exposure," in *Asia–Pacific Electromagn. Compat. Symp./19th Int. Electromagn. Compat. Symp.*, Zurich, Switzerland, May 19–23, 2008, pp. 212–215.

[10] M. Klemm and G. Troester, "EM energy absorption in the human body tissues due to UWB antennas," *Progr. Electromagn. Res.*, vol. 62, pp. 261–280, 2006.

[11] V. De Santis, M. Feliziani, and F. Maradei, "Safety assessment of UWB radio systems for body area network by the FD^{2}TD method," *IEEE Trans. Magn.*, vol. 46, no. 8, pp. 3245–3248, 2010.

[12] Z. N. Chen, A. Cai, T. S. P. See, X. Qing, and M. Y. W. Chia, "Small planar UWB antennas in proximity of the human head," *IEEE Trans. Microw. Theory Techn.*, vol. 54, no. 4, pp. 1846–1857, Apr. 2006.

[13] C. Buccella, V. De Santis, and M. Feliziani, "Prediction of temperature increase in human eyes due to RF sources," *IEEE Trans. Electromagn. Compat.*, vol. 49, no. 4, pp. 825–833, Nov. 2007.

[14] N. I. M. Yusoff, S. Khatun, and S. A. AlShehri, "Characterization of absorption loss for UWB body tissue propagation model," in *IEEE 9th Int. Commun. Conf.*, Kuala Lumpur, Malaysia, Dec. 15–17, 2009, pp. 254–258.

[15] A. Santorelli and M. Popovic, "SAR distribution in microwave breast screening: Results with TWTLTLA wideband antenna," in *7th Int. Intell. Sens., Sens. Networks, Inform. Process. Conf.*, Dec. 6–9, 2011, pp. 11–16.

[16] F. Shahrokhi, K. Abdelhalim, D. Serletis, P. L. Carlen, and R. Genov, "The 128-channel fully differential digital integrated neural recording and stimulation interface," *IEEE Trans. Biomed. Circuits Syst.*, vol. 4, no. 3, pp. 149–161, Jun. 2010.

[17] M. Chae, Z. Yang, M. R. Yuce, L. Hoang, and W. Liu, "A 128-channel 6 mW wireless neural recording IC with spike feature extraction and UWB transmitter," *IEEE Trans. Neural Syst. Rehabil. Eng.*, vol. 17, no. 4, pp. 312–321, Aug. 2009.

[18] "UWB first report and order," FCC, Washington, DC, USA, Tech. Rep. FCC 02-48, 2002.

[19] O. Novak, C. Charles, and R. B. Brown, "A fully integrated 19 pJ/pulse UWB transmitter for biomedical applications implemented in 65 nm CMOS technology," in *IEEE Int. Ultra-Wideband Conf.*, Sep. 14–16, 2011, pp. 72–75.

[20] W.-N. Liu and T.-H. Lin, "An energy-efficient ultra-wideband transmitter with an FIR pulse-shaping filter," in *Int. VLSI Design, Automat., Test Symp.*, Apr. 23–25, 2012, pp. 1–4.

[21] T. Koike-Akino, "SAR analysis in tissues for *in vivo* UWB body area networks," in *IEEE Global Telecommun. Conf.*, Nov. 30–Dec. 4, 2009, pp. 1–6.

[22] P. J. Dimbylow, "Fine resolution calculations of SAR in the human body for frequencies up to 3 GHz," *Phys. Med. Biol.*, vol. 47, no. 16, pp. 2835–2846, 2002.

[23] CST Studio Suite. CST AG, Darmstadt, Germany, 2012. [Online]. Available: www.cst.com

[24] "Compilation of the dielectric properties of body tissues at RF and microwave frequencies," AFOSR/NL Bolling AFB, Washington, DC, USA, Final Rep., Feb. 1996.

[25] S. C. DeMarco, G. Lazzi, W. Liu, J. D. Weiland, and M. S. Humayun, "Computed SAR and thermal elevation in a 0.25-mm 2-D model of the human eye and head in response to an implanted retinal stimulator—Part I: Models and methods," *IEEE Trans. Antennas Propag.*, vol. 51, no. 9, pp. 2274–2285, Sep. 2003.

[26] C. Gabriel, S. Gabriel, and R. W. Lau, "The dielectric properties of biological tissues: I. Literature survey," *Phys. Med. Biol.*, vol. 41, no. 11, pp. 2231–2249, 1996.

[27] S. Gabriel, R. W. Lau, and C. Gabriel, "The dielectric properties of biological tissues: III. Parametric models for the dielectric spectrum of tissues," *Phys. Med. Biol.*, vol. 41, no. 11, pp. 2271–2293, 1996.

[28] A. Peyman, C. Gabriel, E. H. Grant, G. Vermeeren, and L. Martens, "Variation of the dielectric properties of tissues with age: The effect on the values of SAR in children when exposed to walkie-talkie devices," *Phys. Med. Biol.*, vol. 54, no. 2, pp. 227–241, 2009.

[29] C. Gabriel, "Dielectric properties of biological tissue: Variation with age," *Bioelectromagnetics*, vol. 26, no. 7, pp. 12–18, Sep. 2, 2005.

[30] J. Wang, O. Fujiwara, and S. Watanabe, "Approximation of aging effect on dielectric tissue properties for SAR assessment of mobile telephones," *IEEE Trans. Electromagn. Compat.*, vol. 48, no. 2, pp. 408–413, May 2006.

[31] K. Lichtenecker, "Die dielektrizitatskonstante naturlicher und kunstlicher mischkorper," *Phys. Zeit.*, vol. 27, pp. 115–158, 1926.

[32] P. L. Altman and D. S. Dittmer", *Biology Data Book: Blood and Other Body Fluids*. Washington, DC, USA: Fed. Amer. Soc. Experiment. Biol., 1974.

[33] T. Weiland, M. Timm, and I. Munteanu, "A practical guide to 3-D simulation," *IEEE Microw. Mag.*, vol. 9, no. 6, pp. 62–75, 2008.

[34] M. Clement and T. Weiland, "Discrete electromagnetism with finite integral technique," *Progr. Electromagn. Res.*, vol. 32, pp. 65–87, 2001.

[35] *Recommended Practice for Measurements and Computations of Radio Frequency Electromagnetic Fields With Respect to Human Exposure to Such Fields, 100 kHz–300 GHz*, IEEE Standard C95.3, 2002.

[36] "Threshold limit values for chemical substances and physical agents and biological exposure indices," in *Amer. Government. Ind. Hygienists Conf.*, 1996, pp. 0–144.

[37] H. H. Pennes, "Analysis of tissue and arterial blood temperatures in resting forearm," *J. Appl. Physiol.*, vol. 1, pp. 93–122, 1948.

[38] M. Hoque and O. P. Gandhi, "Temperature distributions in the human leg for VLF-VHF exposures at the ANSI recommended safety levels," *IEEE Trans. Biomed. Eng.*, vol. 35, no. 6, pp. 442–449, Jun. 1988.
[39] P. Bernardi, M. Cavagnaro, S. Pisa, and E. Piuzzi, "Specific absorption rate and temperature elevation in a subject exposed in the far-field of radio-frequency sources operating in the 10–900-MHz range," *IEEE Trans. Biomed. Eng.*, vol. 50, no. 3, pp. 295–304, Mar. 2003.
[40] T. Dissanayake, K. P. Esselle, and M. R. Yuce, "Dielectric loaded impedance matching for wideband implanted antennas," *IEEE Trans. Microw. Theory Techn.*, vol. 57, no. 10, pp. 2480–2487, Oct. 2009.
[41] H. Bahrami, B. Gosselin, and L. A. Rusch, "Design of a miniaturized UWB antenna optimized for implantable neural recording systems," in *IEEE 10th Int. New Circuits Syst. Conf.*, Jun. 17–20, 2012, pp. 309–312.
[42] K. Y. Yazdandoost, "UWB antenna for body implanted applications," in *9th Eur. Radar Conf.*, Oct. 31–Nov. 2, 2012, pp. 606–609.
[43] A. Kiourti, M. Christopoulou, and K. S. Nikita, "Performance of a novel miniature antenna implanted in the human head for wireless biotelemetry," in *IEEE Int. Antennas Propag. Symp.*, Jul. 3–8, 2011, pp. 392–395.
[44] K. Jaehoon and Y. Rahmat-Samii, "Implanted antennas inside a human body: Simulations, designs, and characterizations," *IEEE Trans. Microw. Theory Techn.*, vol. 52, no. 8, pp. 1934–1943, Aug. 2004.

Kasun. M. S. Thotahewa (S'12) received the B.Sc. (Hons.) degree in electronic and telecommunications from the University of Moratuwa, Moratuwa, Sri Lanka, in 2008, and is currently working toward the Ph.D. degree at Monash University, Clayton, Vic., Australia.

He was a Network Operations Engineer with one of the major mobile service providers in Sri Lanka.

Jean-Michel Redouté (S'05–M'09–SM'12) received the M.S. degree in electronics from Hogeschool Antwerpen, Antwerpen, Belgium, in 1998, and the M.Eng. degree in electrical engineering from the University of Brussels (VUB), Brussels, Belgium, in 2001.

In August 2001, he joined Alcatel Bell, Antwerp, Belgium, where he was involved in the design of analog microelectronic circuits for telecommunications systems. From January 2005 to August 2009, he was with ESAT-MICAS Laboratories, University of Leuven, as a Ph.D. Research Assistant. In September 2009, he joined the Berkeley Wireless Research Center, University of California at Berkeley, as a Postdoctoral Scholar. In September 2010, he joined Monash University, Clayton, Vic., Australia, as a Senior Lecturer. His research interests include robust mixed-signal integrated-circuit design with a high immunity to electromagnetic interference, electromagnetic compatibility, and exposure, biomedical circuit design, and RF integrated-circuit design.

Mehmet Rasit Yuce (S'01–M'05–SM'10) received the M.S. degree in electrical and computer engineering from the University of Florida, Gainesville, FL, USA, in 2001, and the Ph.D. degree in electrical and computer engineering from North Carolina State University (NCSU), Raleigh, NC, USA, in 2004.

From August 2001 to October 2004, He was a Research Assistant with the Department of Electrical and Computer Engineering, NCSU. In 2005, he was a Post-Doctoral Researcher with the Electrical Engineering Department, University of California at Santa Cruz. From June 2005 to July 2011, he was a Senior Lecturer with the School of Electrical Engineering and Computer Science, University of Newcastle, Newcastle, N.S.W., Australia . In July 2011, he joined the Department of Electrical and Computer Systems Engineering, Monash University, Clayton, Vic., Australia. He has authored or coauthored over 80 technical papers. He authored *Wireless Body Area Networks* (Pan Stanford, 2011). He is an Associate Editor for the *International Journal of Medical Engineering and Informatics*. His research interests include wireless implantable telemetry, WBANs, bio-sensors, microelectromechanical systems (MEMS) sensors, integrated circuit technology dealing with digital, analog, and RF circuit design for wireless, biomedical, and RF applications.

Dr. Yuce is an associate editor for numerous journals, including the IEEE SENSORS JOURNAL. He was the recipient of a 2007 National Aeronautics and Space Administration (NASA) Group Achievement Award for the development of a silicon-on-insulator (SOI) transceiver and a 2010 Research Excellence Award of the Faculty of Engineering and Built Environment, University of Newcastle.